

Antenna Health-Aware Selective Beamforming for Hardware-Constrained DFRC Systems I

Anis Hamadouche, Tharm Ratnarajah, Christos Masouros, John Thompson, and Mathini Sellathurai

Abstract—This paper addresses the optimization challenges in dual-functional radar-communication (DFRC) systems with a focus on array selection and beamforming in dynamic and heterogeneous operational contexts. We propose a novel array selection criterion that integrates antenna health information into the optimization process, distinguishing our approach from traditional methods. Our methodology employs gradient dual ascent and dual proximal-gradient ascent for tackling the constrained non-convex and non-smooth nature of sparse array selection problems. A key feature of our strategy is the implementation of proportional fairness among communication users, which aligns with system resource limitations while meeting the minimum rate requirements for all users. This facet of our method not only enhances system efficiency and responsiveness but also ensures a fair distribution of resources. Through extensive simulations, the efficacy of the proposed solutions in optimizing DFRC system performance is validated, illustrating their applicability in integrated sensing and communication (ISAC) scenarios. Our findings contribute to the evolving field of DFRC systems, offering new perspectives and solutions for the challenges in array selection and beamforming optimisation.

Index Terms—Dual Function Radar Communication (DFRC); Joint Radar-Communication (JRC); Beamforming; 5G; Optimization Algorithms.

I. INTRODUCTION

In the contemporary landscape of cellular networks, the ever-increasing demand for high-speed, reliable communication has ushered in a paradigm shift towards more dynamic and flexible system architectures. Modern cellular networks are no longer static entities; they are vibrant ecosystems that must adapt in real-time to fluctuating user demands, varying network conditions, and stringent quality of service (QoS) requirements. This need for adaptiveness and responsiveness is particularly pronounced in the realm of Dual Function Radar Communication (DFRC) systems, where the convergence of radar and communication functionalities within the same spectral footprint presents unique challenges and opportunities [9, 22, 6, 16, 4].

The adaptiveness in modern cellular networks is crucial for several reasons. Firstly, user requirements are no longer uniform or predictable; they are diverse and dynamic [1, 7, 5, 3, 2]. Users expect seamless connectivity whether they are

streaming high-definition videos, engaging in real-time gaming, or leveraging IoT devices for smart home applications. The network must adapt its resource allocation strategies in real-time to meet these varying demands without compromising on speed, latency, or reliability [2].

Secondly, the operational environment of cellular networks is inherently dynamic. Factors such as user mobility, interference from neighboring cells, and physical obstructions can dramatically alter the network conditions. A responsive network can swiftly adjust its operational parameters, such as beamforming vectors [36, 20, 24, 21, 11, 14], power levels [33, 13, 26, 8, 18], and frequency bands, to mitigate these effects and maintain optimal performance.

In the context of DFRC systems, the need for adaptiveness and responsiveness is further magnified. These systems operate in the high-frequency mmWave bands, known for their vast bandwidth and high data rate potential. However, they also exhibit high sensitivity to obstacles and rapid signal degradation over distance. The dual-functionality of these systems, catering to both radar sensing and wireless communication, adds another layer of complexity. The system must not only manage the communication requirements but also ensure the radar's operational integrity for applications like target detection and tracking.

The introduction of fast algorithms in DFRC systems represents a significant step towards addressing these challenges. By adapting the beamforming weights while incorporating a phased array elements' reliability information, these algorithms ensure that the system can respond in real-time to changes in user requirements, environmental conditions, and structural integrity. This results in a system that is not just reactive but proactive in its approach to maintaining service quality, operational efficiency, and system reliability.

The need for adaptiveness and responsiveness in modern cellular networks, and more specifically in DFRC systems, is not just a requirement; it is a fundamental attribute that defines their operational efficacy and future readiness. As the spectrum of user requirements and operational challenges continues to expand, the ability of these networks to dynamically adapt and respond will remain a critical determinant of their success and sustainability.

Proportional fairness, in its regular sense, has been a staple in communication system design. The objective is to allocate resources in such a way that the allocation to any user can only be increased at the expense of a proportionally larger decrease in the allocation to another user. This principle ensures that each user gets a "fair" portion of the resource, given everyone's requirements.

Anis Hamadouche and Mathini Sellathurai are with the School of Engineering & Physical Sciences, Heriot-Watt University, Edinburgh EH14 4AS, UK (e-mail: {ah225,ah2161,m.sellathurai}@hw.ac.uk). Christos Masouros is with the Institute of Communications and Connected Systems, University College London, UK (e-mail: c.masouros@ucl.ac.uk). Tharm Ratnarajah and John Thompson are with the School of Engineering, University of Edinburgh, Edinburgh, EH9 3BF, UK (e-mail: T.Ratnarajah, jst@ed.ac.uk@ed.ac.uk).

In traditional scenarios, where all users possess the same modulation scheme and Quality of Service (QoS) demands, proportional fairness is effective. It ensures an equitable distribution of resources and, consequently, a balanced user experience across the network.

However, the landscape of communication networks, especially in modern cellular systems, is changing. The introduction of diverse services, such as IoT devices, video streaming, online gaming, and real-time communications, means that users now have different QoS needs. Furthermore, advancements in communication technologies have led to the development of multiple modulation schemes, each with its own set of advantages and limitations. As a result, not every user on the network will be equipped or optimized to handle every modulation scheme.

In such a heterogeneous environment, adhering to traditional proportional fairness can lead to inefficiencies. For example, allocating the same bandwidth to both a high-definition video stream and a simple IoT sensor data transmission can lead to wastage of resources. The video stream might need more bandwidth for a smooth experience, while the IoT data, being less bandwidth-intensive, will underutilize its allocation.

Given these complexities, the concept of utility proportional fairness emerges as a more appropriate solution. Here, the "utility" represents a measure of user satisfaction or the effectiveness of the resource allocation to a user. Instead of ensuring that every user gets an equal share of the resource, utility proportional fairness ensures that every user derives an equal level of satisfaction or utility from their resource allocation. This can translate to different amounts of resources for different users, depending on their QoS demands and modulation capabilities.

In conventional beamforming designs, the distribution of transmission power across the antenna array does not typically account for the varying reliability or condition of individual antenna elements. This oversight can lead to scenarios where power is allocated to compromised or less reliable elements, resulting in suboptimal system performance and increased vulnerability to failures. However, by integrating a phased array elements reliability matrix into the beamforming optimization problem, the system gains the ability to discern the reliability levels of individual elements and adjust its power distribution accordingly.

This integration leads to the emergence of a sparse beamforming matrix, a strategic configuration where the power is not uniformly spread across the entire array but is instead concentrated on elements with higher reliability scores. Such a focused approach ensures that the most dependable elements bear the brunt of the transmission responsibility, significantly enhancing the system's resilience to element failures or degradations. In scenarios of structural damage or progressive wear and tear, this method proves invaluable as it allows the system to dynamically recalibrate its power distribution, continuously adapting to the evolving condition of the antenna array.

The advantages of this approach are manifold. Firstly, it elevates the overall system reliability by effectively bypassing or mitigating the impact of unreliable or damaged elements. Secondly, it enhances fault tolerance, ensuring that the sys-

tem maintains operational integrity and continues to meet performance standards even when certain elements are compromised. This resilience is particularly crucial in scenarios where uninterrupted operation is paramount, such as in critical communication infrastructure or in defense applications.

Furthermore, this method of incorporating structural sparsity knowledge into beamforming design paves the way for more intelligent and adaptive DFRC systems. By allowing the system to self-assess and dynamically adjust to its structural health, it introduces a level of self-awareness and self-optimization, which is a significant stride towards smarter, more autonomous communication systems.

Our contributions in dual-functional radar-communication (DFRC) systems are characterized by:

- The introduction of a new array selection criterion that integrates antenna-health information for beam pattern correction and enhancing system reliability;
- introducing simple, lightweight, optimization techniques like gradient dual ascent and proximal-gradient dual ascent for directly tackling nonconvex challenges in sparse array selection without unnecessary mathematical relaxation;
- ensuring proportional fairness among communication users and radar, aligning with resource constraints and guaranteeing minimum rate requirements. This comprehensive approach not only enhances the system's efficiency and responsiveness but also ensures equitable resource distribution, making it highly relevant for the practical demands of modern DFRC and integrated sensing and communication (ISAC) systems.

The paper is systematically organized into six main sections to provide a comprehensive exploration of the research topic. Section II, "Related Work", lays the foundational groundwork by reviewing pertinent literature, thereby contextualizing our study within the broader scope of existing research in Dual Function Radar Communication (DFRC) systems. In Section III, "Problem Formulation", we formulate the joint radar-communication beamforming problem as an optimisation problem and introduce the mathematical system models, detailing the complexities and setting the stage for the subsequent discussion of our proposed methodologies. In Section IV, "Antenna-Health Aware Beamforming", we introduce the Proximal Gradient Dual Ascent (PGDA) algorithm, emphasizing its adaptiveness and efficiency in managing spectral resources and maintaining system reliability. Section V, "Experimental Results", presents a rigorous evaluation of our proposed solutions, substantiating our theoretical claims with empirical data and insightful analysis. Finally, Section VI, "Conclusion", encapsulates the key findings, discusses the implications of our research, and offers a perspective on potential future directions in the realm of DFRC systems.

II. RELATED WORK

In the domain of hybrid beamforming for dual-functional radar-communication (DFRC) systems, Cheng et al. [16] and Qi et al. [25] have made significant contributions. Cheng et al. proposed a design for multi-carrier DFRC systems,

focusing on optimizing sum-rate under power and similarity constraints. Qi et al. extended these concepts to mmWave MIMO integrated sensing and communication (ISAC) systems, with a focus on designing transmit beams for DFRC base stations and optimizing beam patterns under communication user constraints.

In the optimization of transmit/receive beamforming for MIMO-OFDM based DFRC systems, Tian et al. [19] explored quality of service (QoS) and transmit power constraints, using Kullback-Leibler divergence as design metrics. Liu et al. [12] proposed a MIMO beamforming design aimed at joint radar sensing and multiuser communication, with an objective to minimize the mean squared error (MSE) for target estimation while ensuring user signal-to-interference-plus-noise ratios (SINRs).

Additional advancements in beamforming and system optimization have been presented by Wang et al. [29], Wei et al. [30], and Li et al. [23]. Wang et al. addressed low-complexity beamforming designs in a MIMO radar and multi-user MIMO communication context. Wei et al. investigated an IRS-aided DFRC system, jointly designing radar receive filters, frequency-dependent beamforming, and IRS phases. Li et al. developed an optimization framework for joint transmit beamforming and receive filters design in a two-cell DFRC network.

In predictive beamforming, significant contributions have been made by Yuan et al. [15], Liu et al. [10], and Yu et al. [39]. Yuan et al. developed a predictive beamforming scheme for vehicular networks, aiming to reduce signaling overhead and improve tracking performance. Liu et al. addressed predictive beamforming for V2I links without the need for explicit state evolution models. Yu et al. proposed a neural network-based approach for angle estimation in multi-RSU vehicular networks.

Tian et al. [27] explored adaptive bit/power allocation with beamforming to enhance BER performance in DFRC. Liu et al. [11] focused on radar-assisted predictive beamforming for vehicular links, employing DFRC signals for vehicle tracking.

Cheng et al. [16] and Dai et al. further delved into hybrid beamforming in OFDM-DFRC and SINR metric-based DFRC systems, respectively, addressing nonconvex problems using consensus-ADMM and SDR techniques. Cheng et al. [21] proposed double-phase-shifter based hybrid beamforming for mmWave DFRC systems, tackling nonconvex challenges through consensus-ADMM and WMMSE.

Xu et al. [37] employed learning approaches, particularly neural networks, to optimize transmit beamforming, addressing the nonconvex nature of the problem. Liang and Huang [35] utilized online learning networks for nonconvex joint transmit waveform and receive beamforming design in DFRC systems.

Lastly, Yuan et al. [15] and Yu et al. [39] focused on predictive beamforming for vehicular networks, proposing new algorithms based on Bayesian prediction and neural networks to estimate and predict motion parameters, effectively addressing nonconvex problems.

Addressing nonconvexity in these problems often involves employing advanced optimization techniques such as semidefinite

relaxation (SDR), successive convex approximation (SCA), or majorization-minimization (MM) methods. For instance, Dai et al. [17] use SDR and FPP-SCA techniques to solve their non-convex quadratically constrained quadratic programs. Similarly, Liu et al. [24] employ ADMM and MM methods to tackle their complex non-convex optimization problem.

Recent advancements in dual-functional radar-communication (DFRC) systems have led to innovative approaches in antenna selection and beamforming design. For instance, Xu et al. (2023) [38] delve into sparse array design via antenna selection in joint communication radar systems, focusing on optimizing the ambiguity function for enhanced radar detection and preserving communication quality of service. Their approach features an innovative optimization method that incorporates a genetic algorithm, showcasing its effectiveness through simulation results. Wu et al. (2022) [31] examine antenna selection technology within the realm of massive MIMO systems in 5G networks, highlighting its critical role in augmenting channel capacity and bolstering anti-interference capabilities.

Further contributions in this field include the work of Xu et al. (2022) [32], who propose an approach for optimizing transmit beamforming matrices. Their method aims to balance the radar estimate Cramer-Rao bound (CRB) with the communication rate. Huang et al. (2023) [34] concentrate on designing transmit sparse array beamformers for DFRC systems, integrating radar transmit beamforming with communication capabilities via amplitude and phase modulation. Additionally, Valiulahi et al. (2022) [28] explore antenna selection strategies for energy-efficient mmWave DFRC systems, with a focus on minimizing the CRB for target tracking while ensuring communication quality of service.

Compared to the previously mentioned methods, our approach offers a more holistic and adaptive solution for beamforming and array selection in dual-functional radar-communication (DFRC) systems. Traditional methods, such as those employed by Xu et al. (2023) [38], Wu et al. (2022) [31], and others, often rely on semidefinite relaxation (SDR) and alternating optimization techniques. These methods, while effective, may not fully capture the dynamic nature of DFRC environments and can be computationally intensive.

In contrast, our method incorporates a new array selection criterion that embeds prior information about the DFRC system's health directly into the problem. This approach, employing gradient dual ascent and dual proximal-gradient ascent for sparse array selection, directly tackles the nonconvex challenges inherent in these systems. Our method stands out in its ability to converge faster and adapt more effectively to changing conditions, making it well-suited for real-time applications in dynamic environments.

Furthermore, our solution achieves an optimal balance between radar and communication objectives, ensuring proportional fairness among communication users. This aspect is crucial in scenarios where resource constraints are stringent, and equitable distribution is essential. By guaranteeing a minimum rate requirement for each user, our approach not only maximizes system performance but also ensures fairness

and efficiency across the network.

III. PROBLEM FORMULATION

Consider a millimeter wave (mmWave) Dual-Function Radar Communications (DFRC) node that is equipped with N_t transmit antennas and N_r receive antennas. This node communicates with M users, each equipped with a single antenna, while simultaneously tracking a K point targets. Let us assume \mathbf{X} to be a dual-function narrow-band transmit matrix with dimensions $N_t \times L$,

$$\mathbf{X} = \mathbf{W}\mathbf{S} \quad (1)$$

where $L > N_t$ represents the length of the DFRC signal frames, $\mathbf{W} = [\mathbf{w}_1, \dots, \mathbf{w}_M]^T$ is the DFRC beamforming matrix required to be designed in which \mathbf{w}_j is the j -th beamforming vector and $\mathbf{S} \in \mathbb{C}^{M \times L}$ is the data stream.

We assume that the data streams are independent of each other, thus

$$\frac{1}{L}\mathbf{S}\mathbf{S}^H = \mathbf{I}_{N_t} \quad (2)$$

which asymptotically holds when signaling follows a Gaussian distribution and L is sufficiently large.

Equation (2) indicates that the data streams are orthogonal to each other over the frame's length L , ensuring that they don't interfere with each other. This is a typical assumption in many communication systems to avoid interference between different data streams. The right-hand side \mathbf{I}_{N_t} is the identity matrix of size N_t , implying that when the data streams are correlated with their Hermitian transposes (denoted by \mathbf{S}^H), they produce an identity matrix scaled by the frame's length L .

A. Radar system Model

The matrix \mathbf{Y}^r , which represents the signals reflected by the target and received by the antennas, has dimensions $N_r \times L$.

$$\mathbf{Y}^r = \mathbf{G}\mathbf{X} + \mathbf{\Omega} \quad (3)$$

where $\mathbf{G} \in \mathbb{C}^{N_r \times N_t}$ is the target response matrix and $\mathbf{\Omega} \in \mathbb{C}^{N_r \times L}$ is the additive white Gaussian noise (AWGN) matrix, with a variance σ_r^2 for each entry.

For a collocated MIMO radar, the target response matrix is given by:

$$\mathbf{G} = \sum_{k=1}^K \alpha_k \mathbf{a}(\theta_k) \mathbf{b}^H(\theta_k) \quad (4)$$

Here, α_k denotes the complex coefficient accounting for both the two-way channel amplitude and the radar cross-section of the k -th target. θ_k represents both the angle of departure (AoD) and angle of arrival (AoA) of the k -th target, assuming transmitter and receiver antennas are co-located.

Furthermore, the steering vectors for the transmit and receiver antennas are:

$$\mathbf{a}(\theta) = \left[1, e^{j\frac{2\pi}{\lambda}d\sin(\theta)}, \dots, e^{j\frac{2\pi}{\lambda}d(N_t-1)\sin(\theta)} \right]^T \quad (5)$$

$$\mathbf{b}(\theta) = \left[1, e^{j\frac{2\pi}{\lambda}d\sin(\theta)}, \dots, e^{j\frac{2\pi}{\lambda}d(N_r-1)\sin(\theta)} \right]^T \quad (6)$$

Here, λ denotes the signal's wavelength and d signifies the spacing between antennas.

Let us now discuss the covariance of the radar channel and the mutual information between the received echo signal and the radar channel in the context of MIMO radar systems.

Without loss of generality, in this paper, we assume that $d = \frac{\lambda}{2}$. Consequently, the covariance of the radar channel can be written as:

$$\mathbf{R} = \sum_{k=1}^K \sigma_k^2 (\mathbf{b}(\theta_k) \otimes \mathbf{a}(\theta_k)) (\mathbf{b}(\theta_k) \otimes \mathbf{a}(\theta_k))^H \quad (7)$$

where $\sigma_k^2 = \mathbb{E}[\alpha_k \alpha_k^H]$ denotes the expected strength of the k -th target.

For the radar performance metric, we use the mutual information between the received echo signal and the radar channel, $I(\mathbf{Y}^r; \mathbf{G})$, defined as:

$$I(\mathbf{Y}^r; \mathbf{G}) = H(\mathbf{Y}^r) - H(\mathbf{Y}^r | \mathbf{G}) = \log \det(\mathbf{I}_{N_t} + \sigma_r^{-2} \mathbf{R} \mathbf{X} \mathbf{X}^H) \quad (8)$$

Here, $H(\mathbf{Y}) = P(\mathbf{Y}) \log \int P(\mathbf{Y}) d\mathbf{Y}$ represents the differential entropy of \mathbf{Y} with $P(\mathbf{Y})$ being its probability density function (PDF). Additionally, $H(\mathbf{Y} | \mathbf{G}) = P(\mathbf{Y} | \mathbf{G}) \log \int P(\mathbf{Y} | \mathbf{G}) d\mathbf{Y}$ denotes the conditional differential entropy of \mathbf{Y} given \mathbf{G} . For obtaining (6), the property $\det(\mathbf{I} + \mathbf{A}\mathbf{B}) = \det(\mathbf{I} + \mathbf{B}\mathbf{A})$ is utilized.

In the following subsection, we will introduce the communication model.

B. Communication system model

The received signal $\mathbf{Y}^c \in \mathbb{C}^{M \times L}$ for the single-target case can be represented as:

$$\mathbf{Y}^c = \mathbf{H}^H \mathbf{X} + \mathbf{N}, \quad (9)$$

where $\mathbf{N} \in \mathbb{C}^{M \times L}$ is the AWGN matrix with variance σ_c^2 for each entry. Additionally, $\mathbf{H} = [\mathbf{h}_1, \dots, \mathbf{h}_M] \in \mathbb{C}^{N_t \times M}$ signifies the communication channel matrix where $\mathbf{h}_j \in \mathbb{C}^{N_t}$, $\forall j \in \{1, \dots, M\}$, is the communication channel for the j -th user. The SINR for the m -th user is then given by:

$$\gamma_m = \frac{|\mathbf{h}_m^H \mathbf{w}_m|^2}{\sum_{j \neq m} |\mathbf{h}_m^H \mathbf{w}_j|^2 + \sigma_c^2}, \quad (10)$$

where the term $\sum_{j \neq m} |\mathbf{h}_m^H \mathbf{w}_j|^2$ denotes the interference from other users to the m -th user.

C. Antenna-Health constraints

In a phased array system equipped with N antenna elements and M RF chains, interactions between these components—mediated through beamforming weights, including phase and amplitude adjustments—are captured by a matrix β of dimensions $N \times M$. This matrix encodes the health and operational status of each antenna element in relation to the RF chains. Specifically, each entry $\beta_{i,j}$ within β indicates the reliability or operational health of the connection between the j -th antenna element and the i -th RF chain, with values ranging from 0 (indicative of complete failure or an off state) to 1 (representing a fully operational status). This reliability

metric can aggregate the operational fidelity of individual components, such as power amplifiers, attenuators, phase shifters, or it can directly assess the antenna elements' reliability. In the latter scenario, β simplifies to a vector of length N , where each β'_i , for $i = 1, \dots, N$, quantifies the reliability of the i -th antenna element. Here, N signifies the total number of antenna elements, noted as N_t for transmitters and N_r for receivers.

The determination of system reliability is a complex process involving simulations, far-field and near-field measurements, network analysis, and environmental testing, aimed at understanding and counteracting potential performance degradations. Ongoing surveillance coupled with sophisticated correction algorithms is paramount for ensuring the sustained efficiency and reliability of phased array systems.

The next section elaborates on how to jointly maximise the radar's mutual information and minimum QoS of the communication users subject to power and antenna health constraints.

IV. ANTENNA-HEALTH AWARE BEAMFORMING

In practical implementations, the integration of phased array elements reliability information into the beamforming optimization problem represents a paradigm shift towards more resilient, reliable, and fault-tolerant DFRC systems. This approach not only optimizes the use of the system's resources by focusing power on the most reliable elements but also ensures continuous and efficient operation, even in the face of structural challenges, thereby setting a new standard in the design and operation of advanced communication systems.

A. Antenna-health aware corrective beamforming

Prior information about the phased array structural/connection reliability can be embedded as a structured sparsity into the JRC optimisation problem (11a) as follows:

$$\max_{\mathbf{w}_j, \forall j} \rho_r \log \det \left(\mathbf{I}N_t + \sigma_r^{-2} \mathbf{R} \sum_{j=1}^M \mathbf{w}_j \mathbf{w}_j^H \right) \quad (11a)$$

$$+ \sum_{j=1}^M \rho_j \log(1 + \gamma_j) - \rho_s \sum_{i,j} (1 - \beta_{i,j}) |w_{i,j}|$$

$$\text{s.t.} \quad \text{trace}(\mathbf{w} \mathbf{w}^H) \leq P_t, \quad (11b)$$

$$R_{\min_j} \leq \log(1 + \gamma_j), \forall m. \quad (11c)$$

where we multiply each beamforming element by a corresponding failure mask $\beta_{i,j}$ capturing the reliability of the i -th antenna element to j -th RF chain connection. ρ_s is a regularisation parameter that promotes sparsity and ρ_r, ρ_j are the radar and communication weights, respectively.

Adding the sparsity promoting step yields a nonsmooth nonconvex optimisation problem that can be solved using Algorithm 2, where

$$\lambda^{(k)} \nabla g(\mathbf{x}^{(k_1)}) = \sum_{j=1}^M (\rho_j + \lambda_{1,j}^k - \lambda_{2,j}^k) \log(1 + \gamma_j) \quad (12)$$

and the proximal operator in line 7 can be defined as:

$$\mathbf{z}^{k_1+1} = \arg \min_{\mathbf{x} \in \mathbb{C}^{N_t \times M}} \rho_s \sum_{i,j} (1 - \beta_{i,j}) |x_{i,j}| + \frac{\|\mathbf{x} - \mathbf{x}^{k_1+1}\|_{\mathbf{F}}^2}{2\eta x^{(k_1)}}. \quad (13a)$$

whose solution is given by:

$$z_{i,j}^{(k_1+1)} = \mathcal{S}_\kappa \left(x_{i,j}^{(k_1+1)} \right) \quad (14a)$$

$$= \begin{cases} x_{i,j}^{(k_1+1)} - \kappa, & x_{i,j}^{(k_1+1)} \geq \kappa, \\ 0, & |x_{i,j}^{(k_1+1)}| < \kappa, \\ x_{i,j}^{(k_1+1)} + \kappa, & x_{i,j}^{(k_1+1)} \leq -\kappa, \end{cases} \quad (14b)$$

where $[\cdot]_{i,j}$ stands for the i, j -th matrix element and $\mathcal{S}_\kappa(\cdot)$ is the (elementwise) *soft thresholding* operation with threshold $\kappa = \eta x^{(k_1)} \cdot \rho_s \cdot (1 - \beta_{i,j})$.

Algorithm 1 Group Proximal-Gradient Dual Ascent (GPGDA) For Antenna Selection

- 1: **initialize** \mathbf{w}_j for all j , λ , μ_j for all j , step sizes α and η
 - 2: **while** not converged **do**
 - 3: Compute gradient $\nabla_{\mathbf{w}} \mathcal{L}$
 - 4: Update \mathbf{w} using gradient step: $\mathbf{w} \leftarrow \mathbf{w} + \eta \nabla_{\mathbf{w}} \mathcal{L}$
 - 5: **for** each beamforming row \mathbf{w}_i^r **do**
 - 6: Update group row \mathbf{w}_i^r using the proximal operator:
 - 7: $\mathbf{w}_i^r \leftarrow \text{prox}_{(\rho_s(1-\beta_{i,j}) + \lambda P_A) \|\cdot\|_2}(\mathbf{w}_i^r)$
 - 8: **end for**
 - 9: Update dual variable λ for power constraint:
 - 10: $\lambda \leftarrow \lambda + \alpha \left(\frac{\sum_{j=1}^M \|\mathbf{w}_j^r\|_2^2}{\eta} + P_A \sum_{i=1}^{N_t} \|\mathbf{w}_i^r\|_2 - P_{tot} \right)$
 - 11: **for** each user j **do**
 - 12: Update dual variable μ_j for minimum rate constraint:
 - 13: $\mu_j \leftarrow \mu_j + \alpha (R_{\min_j} - \log(1 + \gamma_j))$
 - 14: **end for**
 - 15: Check for convergence
 - 16: **end while**
-

V. EXPERIMENTAL RESULTS

In this simulation, the primary focus is on a 5G communication model operating within the 28GHz mmWave band, designed to serve four users ($M=4$) in a compact MIMO setting. The system is characterized by a normalized communication channel matrix (\mathbf{H}), originating from a complex Gaussian distribution and normalized by the square root of the number of transmit antennas ($N_t=10$). The transmission process is simulated through a random signal matrix (\mathbf{X}), comprising an optimal beamforming matrix (\mathbf{W}) (to be designed using the PGDA Algorithm) and a randomly generated symbol message. The received signals (\mathbf{Y}^c) incorporate Gaussian noise with a variance of 0.1 (σ_c^2), to mirror practical communication scenarios over 10 signal samples ($S=10$).

Parallel to the communication setup, the radar component, leveraging the same 28GHz mmWave band, operates as a secondary function. It employs a 10×10 antenna array with a half-wavelength antenna spacing ($d=0.011$ meters), focusing

Algorithm 2 Proximal-Gradient Dual Ascent (PGDA) Selective Beamforming

```

1: Initialization:
2: Initialize  $\mathbf{x}^{(0)}$ ,  $\lambda^{(0)}$ ,  $\mu^{(0)}$ , and tol.
3: for  $k = 0, 1, 2, \dots$  until convergence do
4:   x-update using gradient ascent:
5:   while  $L(\mathbf{z}^{(k_1)}, \lambda, \mu) < L(\mathbf{z}^{(k_1-1)}, \lambda, \mu) + \langle \nabla L(\mathbf{z}^{(k_1-1)}, \lambda, \mu), \mathbf{z}^{(k_1)} - \mathbf{z}^{(k_1-1)} \rangle - \frac{1}{2\eta_x} \|\mathbf{z}^{(k_1)} - \mathbf{z}^{(k_1-1)}\|_2^2$  do
6:      $\mathbf{x}^{(k_1+1)} = \mathbf{x}^{(k_1)} + \eta_x \left( \nabla f(\mathbf{x}^{(k_1)}) + \lambda^{(k)} \nabla g(\mathbf{x}^{(k_1)}) - 2\mu^{(k)} \mathbf{x}^{(k_1)} \right)$ 
7:      $\mathbf{z}^{k_1+1} = \text{prox}_{\eta_x^{k_1} \cdot \rho_s \cdot \sum_{i,j} (1-\beta_{i,j}) |w_{i,j}|} \left( \mathbf{x}^{(k_1+1)} \right)$ 
8:      $\eta_x^{(k_1+1)} = \alpha * \eta_x^{(k_1)}$ 
9:   end while
10:   $\mathbf{x}^{(k+1)} = \mathbf{z}^{(k_1+1)}$ 
11:   $\lambda$ - and  $\mu$ -update:
12:   $\lambda_{1,j}^{(k+1)} = \max(0, \lambda_{1,j}^{(k)} - \alpha(R_{\min_j} - g(\mathbf{x}^{(k+1)})))$ 
13:   $\lambda_{2,j}^{(k+1)} = \max(0, \lambda_{2,j}^{(k)} - \alpha(g(\mathbf{x}^{(k+1)})))$ 
14:   $\mu^{(k+1)} = \max(0, \mu^{(k)} - \alpha(\text{trace}(\mathbf{x}^{(k+1)} \mathbf{x}^{(k+1)H}) - P))$ 
15:  if  $\|\mathbf{x}^{(k+1)} - \mathbf{x}^{(k)}\|_2 < \text{tol}$  then
16:    break
17:  end if
18: end for

```

on detecting four targets (K=4) with uniformly distributed angles. The target reflectivities are represented by complex RCS coefficients (alpha), and the radar model incorporates noise with a variance of 0.1 (σ_r^2), identical to the communication model, ensuring uniformity in signal processing across both functionalities.

Assuming a spectrum sharing scenario within the 28GHz band (5G mmWave), a strategic allocation is made where 0.4140 GHz (with a proportion, $\rho_r = 0.0148$), is dedicated to radar usage, while significant portions, specifically 5.6906 GHz, 7.6838 GHz, 7.6128 GHz, and 6.5987 GHz (with respective proportions $\rho = [0.2032, 0.2744, 0.2719, 0.2357]$), are allocated to 5G communication users. This allocation underlines the coexistence strategy of radar and 5G communications in the same frequency band, aiming to optimize the spectrum utilization. The system adheres to strict quality of service (QoS) requirements, ensuring a minimum of 100Mbps and a maximum of 20Gbps data rate for each 5G user within a maximum power budget of 1 kW. This operational framework translates into specific spectral efficiencies, with minimum spectral efficiency denoted as $R_{\min} = [0.0176, 0.0130, 0.0131, 0.0152]$. This structured approach demonstrates a balanced and efficient use of the spectrum, accommodating both radar and multiple 5G users, while meeting the stringent requirements of modern communication systems.

The regularization parameter ρ_s in problem (11a) controls the extent of sparsity and fault tolerance in the solution. Fault tolerance is achieved by embedding prior phased array element's reliability matrix β into problem (11a). In this experiment, the reliability matrix β is depicted below

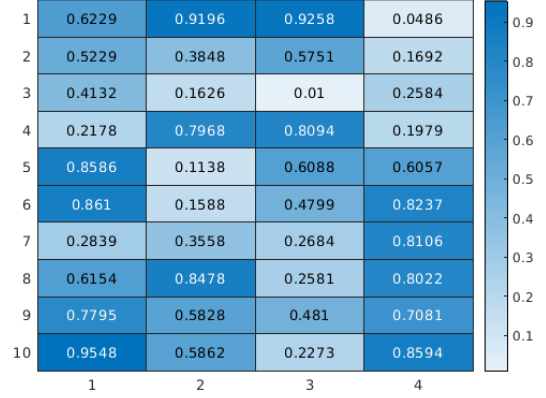


Fig. 1: Array Reliability Matrix

In this experiment, the Proximal Gradient Dual Ascent Algorithm (PGDA) is configured with carefully selected parameters to optimize a communication system with both rate and power constraints. The Lagrangian parameters for minimum rate requirements ($\lambda_{1,j}^0$) and maximum capacity constraints ($\lambda_{2,j}^0$) for each user $j = 1$ to 4 are initialized at 0.04 and 0.06, respectively. The Lagrangian parameter for the power constraint (μ^0) starts at 0.05, ensuring adherence to the system's power budget. The PGDA algorithm operates with a stopping criterion set by a tolerance (tol) of $1e - 12$, guaranteeing precision in convergence. The dual variables are iteratively updated with a learning rate (α) of 0.025 to ensure efficient navigation of the dual space. The primal update learning rate (η_x) is initialised at 0.025 and it is continuously updated using the backtracking line search method with the update parameter (β) is set to 0.5 balancing the speed and stability of convergence in the primal domain. The algorithm is allowed to iterate up to 1000 times, providing ample opportunity for the system to reach an optimal solution within the defined constraints and learning dynamics.

The JRC objective, the radar cost (Mutual Information or MUI) and the aggregated communication cost (sum of spectral efficiencies weighted by bandwidth proportion, i.e., $\sum_{j=1}^M \rho_j \log(1 + \gamma_j)$) are evaluated at every Proximal Gradient Dual Ascent (PGDA) iteration k as shown in the figures below for different sparsity promotion parameter values ρ_s .

The table below illustrates the impact of the sparsity promoting weight ρ_s on the beamforming matrix density (DENS in %), reliability (RL in %) and power consumption (PW in mW) in the DFRC system, alongside its effect on communication spectral efficiency SE_i (bps/Hz), data rate R_i (Gbps) and radar signal mutual information (MUI(Y^r, G)). The summarized results below represent the empirical mean and standard deviation of the performance metrics, derived from 100 run of the aforementioned experiment. Each run commenced with a randomly initialized beamforming weight matrix, ensuring a comprehensive evaluation of the system's performance across a diverse range of starting conditions.

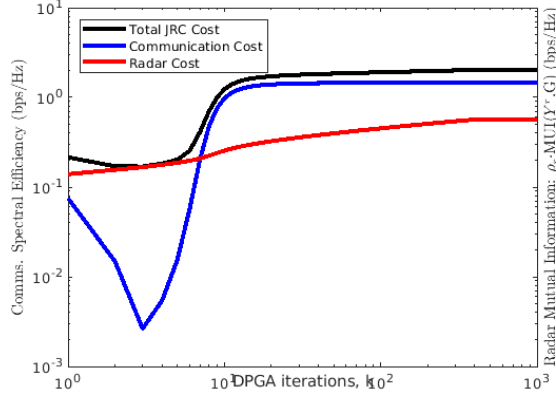


Fig. 2: PGDA Convergence in terms of communication spectral efficiency (bps/Hz) and radar mutual information ($MUI(Y^r, G)$) for 4 targets, 4 users and 10 co-located Tx/Rx antennas with sparsity regularisation term $\rho_s = 0$.

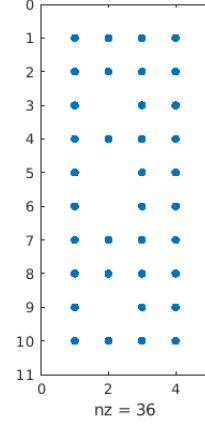


Fig. 4: The corresponding 90%-sparse beamforming weight matrix solution for $\rho_s = 0.7400$.

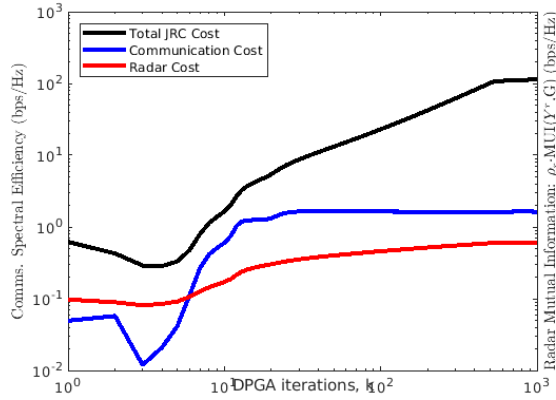


Fig. 3: PGDA Convergence in terms of communication spectral efficiency (bps/Hz) and radar mutual information ($MUI(Y^r, G)$) for 4 targets, 4 users and 10 co-located Tx/Rx antennas with sparsity regularisation term $\rho_s = 0.7400$.

ρ_s	Avg. SE (bps/Hz)	Avg. R (Gbps)	MUI	DENS (%)	PW (mW)	RL (%)
0	1.5149	10.1987	38.2874	100.0000	1.0000	52.4165
0.2218	1.6023	10.8079	39.1305	99.3750	1.0000	52.4565
0.7400	1.7284	11.6534	39.6539	74.2000	1.0001	59.9093
1.3320	1.5675	10.4677	38.2532	51.2750	0.9595	67.1811

TABLE I: Effect of ρ_s on system performance

The analysis of the results reveals a nuanced interplay between the sparsity embedding, indicated by the increase in ρ_s , and various performance metrics of the system, including Spectral Efficiency (SE_i), Data Rate (R_i), Reliability (RL), Power (PW), and Radar Mutual Information (MUI).

As ρ_s increases, the impact on Spectral Efficiency (SE_i) for individual communication users presents a complex pattern. Initially, SE_i experiences an upward trend, suggesting that a moderate level of sparsity embedding enhances the system's spectral efficiency. This could be attributed to the focused allocation of resources, where the system strategically directs power to more reliable and efficient transmission pathways.

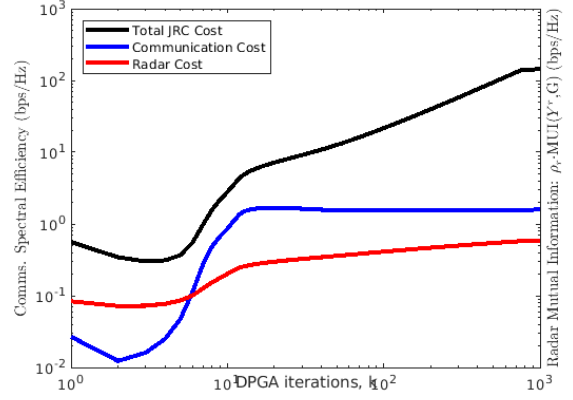


Fig. 5: PGDA Convergence in terms of communication spectral efficiency (bps/Hz) and radar mutual information ($MUI(Y^r, G)$) for 4 targets, 4 users and 10 co-located Tx/Rx antennas with sparsity regularisation term $\rho_s = 1.3308$.

However, this trend does not uniformly persist across all user channels, indicating a nuanced dependency on specific channel conditions and user locations. The variability in standard deviation across different ρ_s values further underlines the complexity of this relationship, emphasizing the influence of channel-specific and environmental factors on spectral efficiency.

In terms of Data Rate (R_i), a similar initial increase is observed with the rise in ρ_s , reflecting the benefits of a more focused and efficient power distribution. This increase aligns with the initial trends in spectral efficiency, suggesting that users are able to leverage the system's resources more effectively. However, the substantial standard deviations, especially at higher ρ_s values, point towards a potential saturation or even a decrease in data rate for certain users. This observation could be indicative of the system reaching its optimization limits, where further sparsity embedding might lead to diminishing returns or necessitate a reevaluation of resource allocation strategies.

The Reliability (RL) of the system shows a clear upward

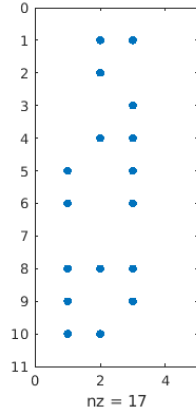


Fig. 6: The corresponding 42.5%-sparse beamforming weight matrix solution for $\rho_s = 1.3308$.

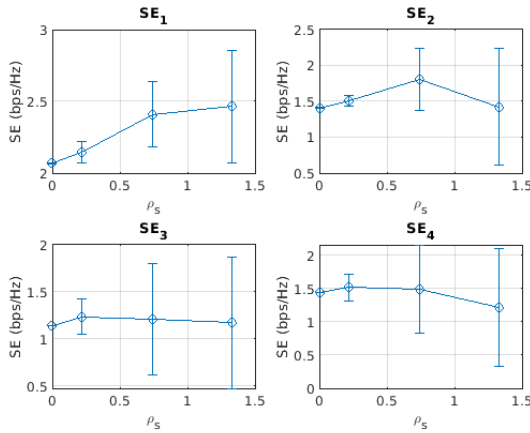


Fig. 7: Spectral Efficiency for Each User vs ρ_s .

trend with increasing ρ_s , underscoring one of the most significant benefits of sparsity embedding. By focusing power on the most reliable elements of the phased array, the system effectively enhances its fault tolerance and operational stability. This improvement in reliability is crucial for maintaining com-

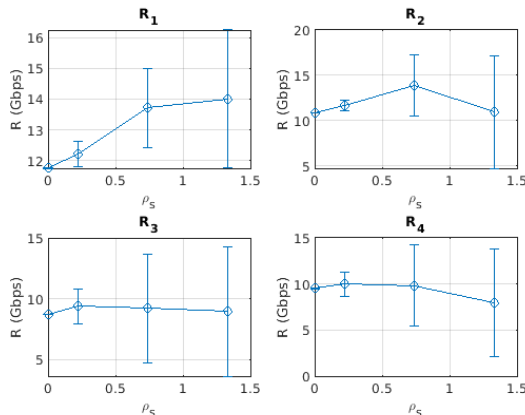


Fig. 8: Data Rate for Each User vs ρ_s .

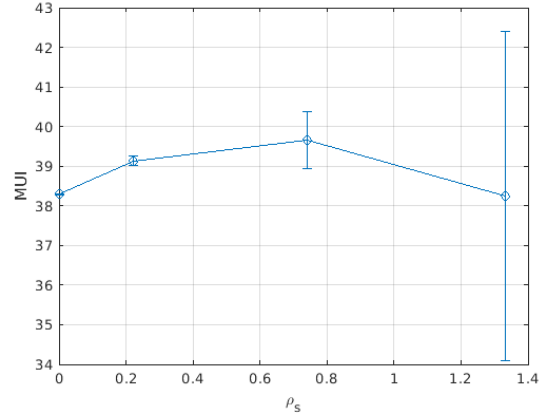


Fig. 9: Radar Mutual Information vs ρ_s .

munication quality, especially in environments where system robustness is paramount.

Interestingly, the Power (PW) usage remains relatively stable across different levels of ρ_s , with only minor fluctuations. This stability is a positive indication that the system manages to enhance its spectral and data rate efficiencies, as well as reliability, without incurring additional power costs. The slight variations and the associated standard deviations suggest that while the system is power-efficient, there might be room for further optimization, especially in terms of power distribution and management.

Finally, the Radar Mutual Information (MUI) presents a nuanced behavior as ρ_s increases. MUI is generally expected to increase with better target detection capabilities, which are influenced by the system's beamforming strategy and the level of sparsity embedding. The observed trends and variations in MUI with different ρ_s values suggest a complex relationship, potentially pointing towards a trade-off between enhancing communication-focused metrics (like SE and R) and maintaining or improving radar detection capabilities. The variations in MUI underscore the need for a balanced approach in DFRC systems, where the dual objectives of communication and radar functionalities must be carefully aligned to ensure optimal overall performance.

Figure 10 illustrates the effect of varying sparsity levels (ρ_s) on the power patterns of defective antennas, juxtaposed with the ideal beampattern (depicted in blue). As ρ_s increases, indicating a selection of more reliable antennas, there is a noticeable improvement in the power pattern of the defective antennas, shown in red. This trend highlights how the strategic selection of antennas can mitigate the adverse impacts of defects. Notably, with higher values of ρ_s , the defective antenna's power pattern progressively aligns with that of the ideal beampattern, showcasing only minimal deviations. This convergence suggests that, despite the presence of defects, it is possible to closely approximate the ideal antenna performance through judicious antenna selection based on sparsity levels, thereby ensuring the integrity of the beampattern is maintained even in the face of antenna imperfections.

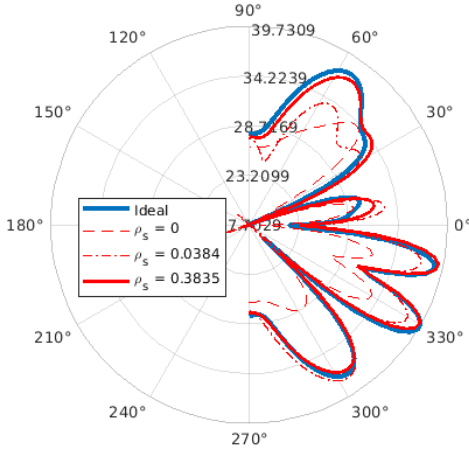


Fig. 10: Superimposed defective antenna’s power patterns (red) for different sparsity levels (ρ_s) on the ideal beampattern (blue).

A. Dynamic data rate requirement

In this experiment, we demonstrate the adaptiveness of the algorithm to varying data rate requirements by simulating a dynamic environment. This is achieved by conducting three iterations, with each iteration featuring a 10% increment in the spectral efficiency for each user. This setup effectively models the changing demands typical in real-world scenarios. We invoke PGDA for this purpose (without sparsity embedding, i.e., $\rho_s = 0$), with its maximum iterations capped at 1000 for the inner iterations. The resulting data, showcasing the dynamic shifts in data rates and radar Mutual Information (MUI), are presented below to illustrate the algorithm’s responsiveness to these evolving spectral efficiency conditions.

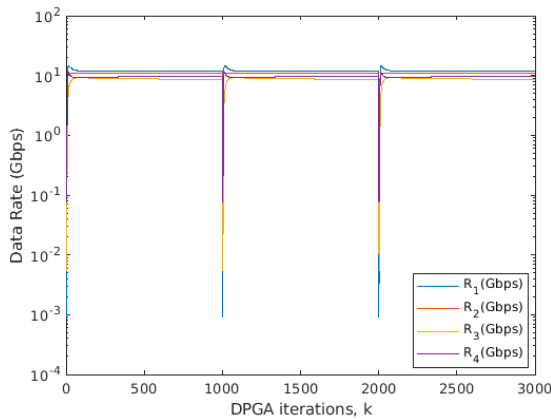


Fig. 11: Dynamic response of PGDA in terms of individual users data rates to changing minimum requirements.

The plots in Figure 11 effectively demonstrate the rapid and efficient response of the PGDA to evolving data rate requirements. Across the iterations, the algorithm successfully maintains a high average data rate for each user: 11.7451 Gbps for User 1, 10.7783 Gbps for User 2, 8.6458 Gbps for User 3, and 9.3761 Gbps for User 4. These rates are

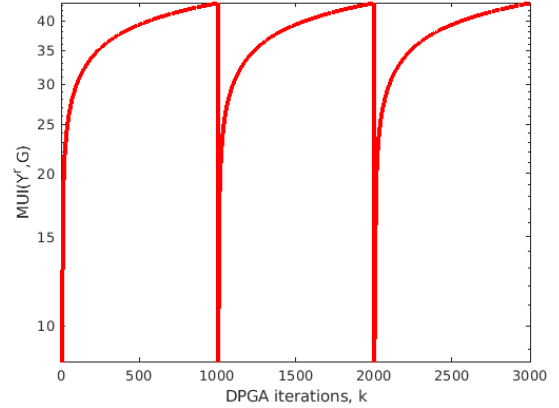


Fig. 12: Dynamic response of PGDA in terms of radar MUI to changing requirements.

significantly above the minimum requirement of 3.1948 Gbps, as observed in the final iteration, while also staying well within the upper limit of 20 Gbps for the data links’ capacity. This performance indicates not only the algorithm’s adaptability to changing conditions but also its capability to efficiently utilize the available spectrum, ensuring that each user experiences high-quality service without exceeding the system’s maximum capacity constraints.

In summary, the enhancement of sparsity embedding (ρ_s) in the DFRC system intricately influences its performance metrics, striking a delicate balance between the enhancement of individual metrics and the sustenance of overall system performance. The empirical results not only underscore the capability of sparsity embedding to elevate system efficiency and reliability but also reveal the complexities and challenges inherent in optimizing a system that concurrently supports radar and communication functionalities. Additionally, the plots vividly demonstrate the PGDA prompt and effective adaptability to changing data rate requirements. The algorithm consistently maintains average data rates for each user well above the minimum requirement and comfortably below the maximum capacity of the data links, exemplifying its proficiency in managing dynamic conditions while optimizing spectrum utilization and ensuring high-quality service for all users.

B. Antenna-health aware selection

In this experiment we use the reliability of antenna elements of Figure 13 to guide the selective beamforming optimisation algorithm to select the most reliable antenna elements subject to a minimum communication rate of 100 Mbps and a total power budget of 100 Watts with power efficiency of 0.4 and per-antenna element power of $P_A = 5$ Watts (for simplicity). Table II summarises the results of our experiments and the antenna selection (non-zero rows) is depicted in Figures 14-15 for different sparsity promotion weights (ρ_s).

The results of Table II suggests an interplay between spectral efficiency (SE), system reliability, and detection capabilities. As ρ_s increases, the general trend in average SE shows

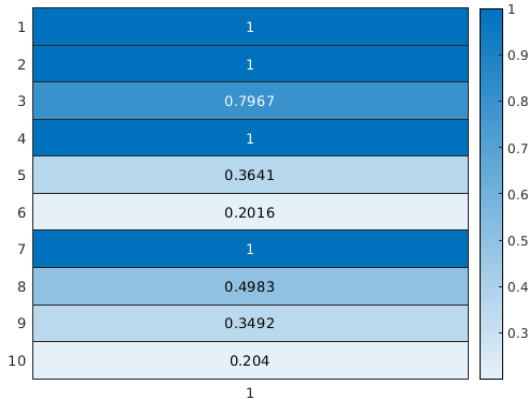


Fig. 13: Linear Array Antenna Reliability Vector

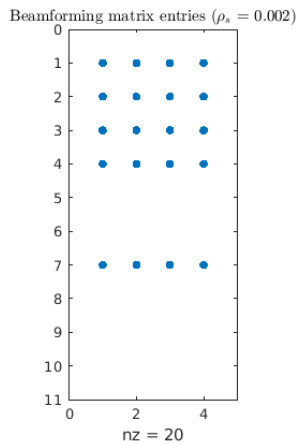


Fig. 14: 50%-sparse beamforming weight matrix solution for $\rho_s = 0.001$.

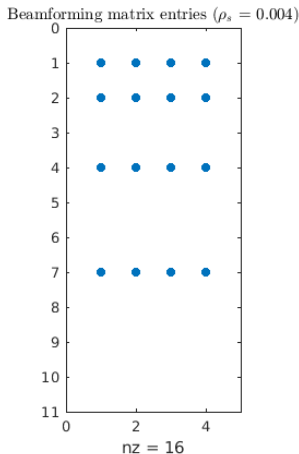


Fig. 15: 40%-sparse beamforming weight matrix solution for $\rho_s = 0.002$.

ρ_s	Avg. SE (bps/Hz)	Avg. R (Gbps)	RL (%)	MUI	DENS (%)	PW (mW)
0	0.1941	1.2763	0.21	22.5190	100	100.0283
0.0008	0.3202	2.0597	1.02	21.8759	90	94.4355
0.0015	0.4827	3.2399	79.67	21.4898	50	97.6907
0.0023	0.3159	2.4701	79.67	21.4933	50	100.0094
0.0031	0.3854	4.3085	79.67	21.4140	50	99.9730
0.0038	0.5033	5.0732	100.0	21.3089	40	100.0466
0.0061	0.1987	1.6519	100.0	21.3097	40	99.9578
0.0767	0.2621	0.9520	100.0	21.3121	40	100.0029

TABLE II: Summary of System Performance Metrics

a peak before declining, suggesting that there exists an optimal sparsity level that maximises communication efficiency without compromising the effectiveness of the hardware. Mutual information MUI (equivalent to detection probability) shows a general decrease with increasing ρ_s , which may at first glance seem counterintuitive. However, this reflects a sophisticated balance: optimizing for reduced hardware usage and enhanced system reliability does not necessarily align with maximizing detection probability, indicating potential trade-offs in radar performance.

Furthermore, the reliability level of 100% achieved at $\rho_s = 0.0038$ value and maintained thereafter highlights how sparsity optimisations can improve the robustness of the system. The decrease in density (DENS) with increasing ρ_s aligns with the strategic goal of reducing active components, underlining the importance of efficient antenna utilisation. The variation in power consumption (PW) at different ρ_s levels - initially decreasing, then slightly increasing - further illustrates the complexity of achieving energy efficient operation while trying to maintain or improve radar detection capabilities and communication quality. This analysis underscores the inherent trade-offs present in JRC system optimisation: While aiming for minimal hardware engagement and enhanced energy efficiency, one must carefully balance these goals against the imperative to sustain or improve radar detection probabilities and overall system performance.

VI. CONCLUSION

In this work, we delved into the intricacies of a Dual Function Radar Communication (DFRC) system operating within the 5G mmWave band at 28GHz, emphasizing a sophisticated beamforming strategy designed to ensure proportional fairness and optimize spectrum sharing among multiple users. The integration of prior knowledge regarding the reliability of phased array elements into the beamforming matrix allows the system to strategically direct transmission power towards the most dependable antenna elements. This not only bolsters overall system reliability and fault tolerance but also aligns with stringent power constraints and quality of service (QoS) requirements. Consequently, it secures both minimum and maximum data rates for 5G communication users. Moreover, the system's capacity for sparsity embedding (ρ_s) intricately impacts its performance metrics, presenting a nuanced balance between the enhancement of individual metrics and the sustenance of overall system performance. The implementation of the Proximal Gradient Dual Ascent (PGDA) algorithm further exemplifies the system's adaptability, maintaining user data rates well within the operational thresholds and demonstrating a rapid, effective response to changing requirements. This

robust operational framework not only accommodates structural complexities but also heralds a significant advancement towards the realization of more intelligent, adaptive, and resilient communication systems.

APPENDIX

A. Gradient of radar detection mutual information term

To find the gradient of $A(X) = \log \det(I_{N_t} + \sigma_r^{-2} R X X^H)$ with respect to X , we can utilize the matrix derivative identity:

$$\frac{\partial \log \det(F(X))}{\partial X} = F(X)^{-1} \frac{\partial F(X)}{\partial X}$$

Given:

$$A(X) = \log \det(Y)$$

where $Y = I_{N_t} + \sigma_r^{-2} R X X^H$,

Let us differentiate $A(X)$ with respect to the matrix X :

$$\frac{\partial A(X)}{\partial X} = \text{trace} \left(Y^{-1} \frac{\partial Y}{\partial X} \right)$$

Now, differentiating Y with respect to X :

$$\frac{\partial Y}{\partial X} = \sigma_r^{-2} R \frac{\partial (X X^H)}{\partial X}$$

Considering $X X^H$, the derivative w.r.t. X would introduce a term that depends on X^H . Therefore, using the identity for differentiation of a product:

$$\frac{\partial (X X^H)}{\partial X} = X^H$$

Combining the above expressions:

$$\frac{\partial A(X)}{\partial X} = \text{trace} (Y^{-1} \sigma_r^{-2} R X^H)$$

This gives the gradient of $A(X)$ with respect to X .

If we want to differentiate the outer product of $\mathbf{w}(1:M)$ with its Hermitian transpose, i.e.,

$$\mathbf{w}(1:M) \mathbf{w}^H(1:M)$$

with respect to a specific element product $w_i w_k^*$, let us derive that.

Let us first note what the matrix product looks like:

$$\mathbf{w}(1:M) \mathbf{w}^H(1:M) = \begin{bmatrix} |w_1|^2 & w_1 w_2^* & \dots & w_1 w_M^* \\ w_2 w_1^* & |w_2|^2 & \dots & w_2 w_M^* \\ \vdots & \vdots & \ddots & \vdots \\ w_M w_1^* & w_M w_2^* & \dots & |w_M|^2 \end{bmatrix}$$

We are interested in the gradient with respect to the element $w_i w_k^*$ (where i and k are given indices).

The only places in this matrix where w_i and w_k^* multiply together are in the (i,k) and (k,i) positions. Everywhere else, differentiating with respect to $w_i w_k^*$ will give zero.

Differentiating the (i,k) position:

$$\frac{\partial (w_i w_k^*)}{\partial (w_i w_k^*)} = 1$$

Because the element in (i,k) is $w_i w_k^*$.

Differentiating the (k,i) position:

$$\frac{\partial (w_k w_i^*)}{\partial (w_i w_k^*)} = 1$$

Because the element in (k,i) is $w_k w_i^*$, which is the conjugate of $w_i w_k^*$, and its derivative with respect to $w_i w_k^*$ is also 1.

For all other positions in the matrix, the derivative is zero.

So, the matrix of derivatives (or the Jacobian) for the element $w_i w_k^*$ is:

$$\frac{\partial \mathbf{w}(1:M) \mathbf{w}^H(1:M)}{\partial (w_i w_k^*)} = \begin{bmatrix} 0 & \dots & 0 & \dots & 0 \\ \vdots & \ddots & \vdots & \ddots & \vdots \\ 0 & \dots & 1 & \dots & 0 \\ \vdots & \ddots & \vdots & \ddots & \vdots \\ 0 & \dots & 0 & \dots & 0 \end{bmatrix}$$

Where the only non-zero entries are at the (i,k) and (k,i) positions, which are both 1.

B. Gradient of communication term

Let us use the gradient ascent for the \mathbf{x} -update. To find the partial derivative of $\sum_{m=1}^M \log(1 + \gamma_m)$ with respect to $w_{i,k}$, we will use the chain rule. Given that γ_m has a specific functional form in terms of $w_{i,k}$, we can express the derivative as:

$$\frac{\partial \sum_{m=1}^M \log(1 + \gamma_m)}{\partial w_{i,k}} = \sum_{m=1}^M \frac{1}{1 + \gamma_m} \frac{\partial \gamma_m}{\partial w_{i,k}} \quad (15)$$

where

$$\frac{\partial \gamma_m}{\partial w_{i,k}} = \begin{cases} \frac{\mathbf{h}_m \mathbf{h}_m^H \mathbf{w}_m + \mathbf{h}_m \mathbf{h}_m^H \mathbf{w}_m^*}{\sum_{j \neq m} |\mathbf{h}_m^H \mathbf{w}_j|^2 + \sigma_c^2} & \text{if } i = m \\ \frac{|\mathbf{h}_m^H \mathbf{w}_m|^2 \mathbf{h}_m \mathbf{h}_m^H \mathbf{w}_i + \mathbf{h}_m \mathbf{h}_m^H \mathbf{w}_i^*}{(\sum_{j \neq i} |\mathbf{h}_i^H \mathbf{w}_j|^2 + \sigma_c^2)^2} & \text{if } i \neq m \end{cases} \quad (16)$$

or

$$\frac{\partial \gamma_m}{\partial w_{i,k}} = \begin{cases} \frac{\mathbf{h}_m \mathbf{h}_m^H \mathbf{w}_m + \mathbf{h}_m \mathbf{h}_m^H \mathbf{w}_m^*}{\sum_{j \neq m} |\mathbf{h}_m^H \mathbf{w}_j|^2 + \sigma_c^2} & \text{if } i = m \\ \gamma_m \frac{\mathbf{h}_m \mathbf{h}_m^H \mathbf{w}_i + \mathbf{h}_m \mathbf{h}_m^H \mathbf{w}_i^*}{\sum_{j \neq i} |\mathbf{h}_i^H \mathbf{w}_j|^2 + \sigma_c^2} & \text{if } i \neq m \end{cases} \quad (17)$$

C. Power Consumption Model for Phased Array Systems

Designing an energy-efficient phased array system for simultaneous radar and communication functionalities demands a comprehensive understanding and integration of a detailed power consumption model. This model incorporates the efficiency of power amplifiers (PAs), the consumption characteristics of digital-to-analog converters (DACs), and the overall energy requirements of RF chain components, alongside the aggregate transmit power. Specifically, the total transmit power (P) is quantified as the sum of the squared magnitudes of the beamforming weights (w_k) for each user, mathematically expressed as

$$P = \sum_{k=1}^M \|w_k\|_2^2. \quad (18)$$

The power output of PAs, crucial for amplifying the transmitted signals, is directly tied to the transmit power and PA efficiency (η), with

$$P_{PA} = \frac{P}{\eta}. \quad (19)$$

DACs, essential for converting digital signals into analog, consume power as a function of their resolution (q), sampling rate (f), and specific power consumption coefficients (c_1 for static and c_2 for dynamic consumption), resulting in

$$P_{DAC} = c_1 f q + c_2 2^q. \quad (20)$$

Additionally, the power consumption attributable to RF chain components, including mixers (P_M), low-pass filters (P_{LF}), and hybrids with buffers (P_{HB}), sums up to

$$P_{RF} = 2P_M + 2P_{LF} + P_{HB}. \quad (21)$$

Consequently, the total power consumption at the base station (P_{tot}) encapsulates the contributions from the PAs, DACs, and RF components across all N_t antenna elements, following

$$P_{tot} = P_{PA} + N_t(2P_{DAC} + P_{RF}). \quad (22)$$

By strategically selecting parameters such as beamforming weights, DAC resolution, and RF chain components, the model facilitates an optimized design of phased array systems that adeptly balances superior performance, exemplified by optimal SINR, with reduced energy consumption, thereby championing sustainable and economically efficient operations.

D. Group Proximal-Gradient Dual Ascent (GPGDA) For Antenna Selection

To solve the given constrained optimization problem using the proximal-gradient dual ascent method, we first formulate the Lagrangian \mathcal{L} to incorporate both the objective function and the constraints. This method iteratively updates the primal variables (the decision variables \mathbf{w}_j for all j) using proximal-gradient steps for the non-smooth part of the Lagrangian, while the dual variables (λ for the power constraint and μ_j for the minimum rate constraints) are updated using gradient ascent steps to handle the constraints.

The Lagrangian for the given optimization problem integrates the objective function, the power consumption constraint, and the minimum rate constraint as follows:

$$\begin{aligned} \mathcal{L}(\mathbf{w}_j, \lambda, \mu_j) := & \rho_r \log \det \left(\mathbf{I}_{N_t} + \sigma_r^{-2} \mathbf{R} \sum_{j=1}^M \mathbf{w}_j \mathbf{w}_j^H \right) \\ & - \rho_s \sum_{i=1}^{N_t} (1 - \beta'_i) \|\mathbf{w}_i^r\|_2 \\ & + \lambda \left(\frac{\sum_{j=1}^M \|\mathbf{w}_j^c\|_2^2}{\eta} + P_A \sum_{i=1}^{N_t} \|\mathbf{w}_i^r\|_2 - P_{tot} \right) \\ & + \sum_{j=1}^M \mu_j (R_{\min_j} - \log(1 + \gamma_j)), \end{aligned} \quad (23a)$$

where ρ_r and ρ_s are the weighting factors for the radar performance and sparsity terms, respectively. \mathbf{w}_j denotes the beamforming vector for the j -th user. \mathbf{w}_i^r and \mathbf{w}_j^c represent the beamforming vectors corresponding to the i -th row and j -th column of the beamforming matrix, respectively. λ and μ_j are the dual variables associated with the power constraint and the minimum rate constraints, respectively.

The optimization process is divided into two main steps:

For the primal variable update, we focus on the non-differentiable part of the Lagrangian, particularly the sparsity-inducing term involving ρ_s . The proximal-gradient step updates the beamforming as follows:

$$\begin{aligned} \mathbf{w}^{(new)} = & \text{prox}_{(\rho_s(1-\beta'_i)+\lambda P_A)\|\cdot\|_2} \left(\mathbf{w}^{(old)} + \eta \nabla_{\mathbf{w}} \mathcal{L}(\mathbf{w}^{(old)}, \lambda, \mu_j) \right), \end{aligned} \quad (24)$$

where η is the step size, and $\nabla_{\mathbf{w}_j} \mathcal{L}(\mathbf{w}_j, \lambda, \mu_j)$ is the gradient of the differentiable part of the Lagrangian with respect to \mathbf{w}_j , and $\text{prox}_{(\rho_s(1-\beta'_i)+\lambda P_A)\|\cdot\|_2}$ is defined as:

$$\begin{aligned} \text{prox}_{(\rho_s(1-\beta'_i)+\lambda P_A)\|\cdot\|_2}(\mathbf{w}_i^r) = & \max \left(1 - \frac{\alpha(\rho_s(1-\beta'_i) + \lambda P_A)}{\|\mathbf{w}_i^r\|_2}, 0 \right) \mathbf{w}_i^r \end{aligned} \quad (25)$$

The dual variables are updated using gradient ascent to enforce the constraints. For the power constraint, the update rule is:

$$\lambda^{(new)} = \lambda^{(old)} + \alpha \left(\frac{\sum_{j=1}^M \|\mathbf{w}_j^c\|_2^2}{\eta} + P_A \sum_{i=1}^{N_t} \|\mathbf{w}_i^r\|_2 - P_{tot} \right),$$

and for the minimum rate constraints:

$$\mu_j^{(new)} = \mu_j^{(old)} + \alpha (R_{\min_j} - \log(1 + \gamma_j)),$$

where α is the step size for the dual variable updates.

REFERENCES

- [1] ETP NetWorld2020 et al. "5g: Challenges, research priorities, and recommendations". In: *Joint White Paper September* (2014).
- [2] Songlin Sun et al. "An intelligent SDN framework for 5G heterogeneous networks". In: *IEEE Communications Magazine* 53.11 (2015), pp. 142–147.
- [3] Ian F Akyildiz et al. "5G roadmap: 10 key enabling technologies". In: *Computer Networks* 106 (2016), pp. 17–48.
- [4] Elie BouDaher et al. "Towards a dual-function MIMO radar-communication system". In: *2016 IEEE Radar Conference (RadarConf)*. IEEE, 2016, pp. 1–6.
- [5] I Chih-Lin et al. "5G: Rethink mobile communications for 2020+". In: *Philosophical Transactions of the Royal Society A: Mathematical, Physical and Engineering Sciences* 374.2062 (2016), p. 20140432.

- [6] Aboulnasr Hassanien et al. “Non-coherent PSK-based dual-function radar-communication systems”. In: *2016 IEEE Radar Conference (RadarConf)*. IEEE. 2016, pp. 1–6.
- [7] Mansoor Shafi et al. “5G: A tutorial overview of standards, trials, challenges, deployment, and practice”. In: *IEEE journal on selected areas in communications* 35.6 (2017), pp. 1201–1221.
- [8] Ammar Ahmed, Yimin D. Zhang, and Braham Himed. “Distributed Dual-Function Radar-Communication MIMO System with Optimized Resource Allocation”. In: *2019 IEEE Radar Conference (RadarConf)*. 2019, pp. 1–5. DOI: 10.1109/RADAR.2019.8835674.
- [9] Aboulnasr Hassanien et al. “Dual-function radar communication systems: A solution to the spectrum congestion problem”. In: *IEEE Signal Processing Magazine* 36.5 (2019), pp. 115–126.
- [10] Fan Liu and Christos Masouros. “A tutorial on joint radar and communication transmission for vehicular networks—Part III: Predictive beamforming without state models”. In: *IEEE Communications Letters* 25.2 (2020), pp. 332–336.
- [11] Fan Liu et al. “Radar-assisted predictive beamforming for vehicular links: Communication served by sensing”. In: *IEEE Transactions on Wireless Communications* 19.11 (2020), pp. 7704–7719.
- [12] Xiang Liu et al. “Joint transmit beamforming for multiuser MIMO communications and MIMO radar”. In: *IEEE Transactions on Signal Processing* 68 (2020), pp. 3929–3944.
- [13] Chenguang Shi et al. “Joint Optimization of Subcarrier Selection and Power Allocation for Dual-Functional Radar-Communications System”. In: *2020 IEEE 11th Sensor Array and Multichannel Signal Processing Workshop (SAM)*. 2020, pp. 1–5. DOI: 10.1109/SAM48682.2020.9104262.
- [14] Weijie Yuan et al. “Bayesian predictive beamforming for vehicular networks: A low-overhead joint radar-communication approach”. In: *IEEE Transactions on Wireless Communications* 20.3 (2020), pp. 1442–1456.
- [15] Weijie Yuan et al. “Joint radar-communication-based bayesian predictive beamforming for vehicular networks”. In: *2020 IEEE Radar Conference (RadarConf20)*. IEEE. 2020, pp. 1–6.
- [16] Ziyang Cheng, Zishu He, and Bin Liao. “Hybrid beamforming design for OFDM dual-function radar-communication system”. In: *IEEE Journal of Selected Topics in Signal Processing* 15.6 (2021), pp. 1455–1467.
- [17] Yuanzhe Dai et al. “Hybrid beamforming for DFRC system based on SINR performance metric”. In: *2021 IEEE/CIC International Conference on Communications in China (ICCC Workshops)*. IEEE. 2021, pp. 82–87.
- [18] Chenguang Shi et al. “Joint Optimization Scheme for Subcarrier Selection and Power Allocation in Multicarrier Dual-Function Radar-Communication System”. In: *IEEE Systems Journal* 15.1 (2021), pp. 947–958. DOI: 10.1109/JSYST.2020.2984637.
- [19] Tuanwei Tian et al. “Transmit/receive beamforming for MIMO-OFDM based dual-function radar and communication”. In: *IEEE Transactions on Vehicular Technology* 70.5 (2021), pp. 4693–4708.
- [20] Li Chen et al. “Generalized transceiver beamforming for DFRC with MIMO radar and MU-MIMO communication”. In: *IEEE Journal on Selected Areas in Communications* 40.6 (2022), pp. 1795–1808.
- [21] Ziyang Cheng et al. “Double-phase-shifter based hybrid beamforming for mmwave DFRC in the presence of extended target and clutters”. In: *IEEE Transactions on Wireless Communications* (2022).
- [22] Jeremy Johnston et al. “MIMO OFDM dual-function radar-communication under error rate and beam pattern constraints”. In: *IEEE Journal on Selected Areas in Communications* 40.6 (2022), pp. 1951–1964.
- [23] Yiqing Li and Miao Jiang. “Joint Transmit Beamforming and Receive Filters Design for Coordinated Two-Cell Interfering Dual-Functional Radar-Communication Networks”. In: *IEEE Transactions on Vehicular Technology* 71.11 (2022), pp. 12362–12367.
- [24] Rang Liu et al. “Joint transmit waveform and passive beamforming design for RIS-aided DFRC systems”. In: *IEEE Journal of Selected Topics in Signal Processing* 16.5 (2022), pp. 995–1010.
- [25] Chenhao Qi et al. “Hybrid beamforming for millimeter wave MIMO integrated sensing and communications”. In: *IEEE Communications Letters* 26.5 (2022), pp. 1136–1140.
- [26] Tuanwei Tian et al. “Adaptive Bit/Power Allocation With Beamforming for Dual-Function Radar-Communication”. In: *IEEE Wireless Communications Letters* 11.6 (2022), pp. 1186–1190. DOI: 10.1109/LWC.2022.3160674.
- [27] Tuanwei Tian et al. “Adaptive bit/power allocation with beamforming for dual-function radar-communication”. In: *IEEE Wireless Communications Letters* 11.6 (2022), pp. 1186–1190.
- [28] Iman Valiulahi et al. “Antenna Selection for Energy-Efficient Dual-Functional Radar-Communication Systems”. In: *IEEE Wireless Communications Letters* 11.4 (2022), pp. 741–745. DOI: 10.1109/LWC.2022.3142043.
- [29] Zhiqin Wang et al. “Low-complexity Transceiver Beamforming for DFRC with MIMO Radar and MU-MIMO Communication”. In: *2022 International Wireless Communications and Mobile Computing (IWCMC)*. IEEE. 2022, pp. 32–37.
- [30] Tong Wei et al. “Simultaneous active-passive beamformer design in IRS-enabled multi-carrier DFRC system”. In: *2022 30th European Signal Processing Conference (EUSIPCO)*. IEEE. 2022, pp. 1007–1011.
- [31] Tongcai Wu, Lina Yuan, and Anran Zhou. “Antenna Selection Technology Research in Massive MIMO System”. In: *2022 IEEE Asia-Pacific Conference on Image*

- Processing, Electronics and Computers (IPEC)*. 2022, pp. 967–970. DOI: 10.1109/IPEC54454.2022.9777612.
- [32] Zhaoyi Xu, Fan Liu, and Athina Petropulu. “Cramér-Rao Bound and Antenna Selection Optimization for Dual Radar-Communication Design”. In: *ICASSP 2022 - 2022 IEEE International Conference on Acoustics, Speech and Signal Processing (ICASSP)*. 2022, pp. 5168–5172. DOI: 10.1109/ICASSP43922.2022.9747651.
- [33] Li Chen et al. “Full-Duplex SIC Design and Power Allocation for Dual-Functional Radar-Communication Systems”. In: *IEEE Wireless Communications Letters* 12.2 (2023), pp. 252–256. DOI: 10.1109/LWC.2022.3222197.
- [34] Jiayi Huang et al. “Transmit Sparse Array Beamformer Design for Dual-Function Radar Communication Systems”. In: *2023 IEEE International Radar Conference (RADAR)*. 2023, pp. 1–6. DOI: 10.1109/RADAR54928.2023.10371099.
- [35] Hao Liang and Bin Liao. “Robust Hybrid Beamforming for MIMO-ISAC System with CSI Imperfection”. In: *2023 6th International Conference on Information Communication and Signal Processing (ICICSP)*. 2023, pp. 665–669. DOI: 10.1109/ICICSP59554.2023.10390724.
- [36] Bin Liao, Xue Xiong, and Zhi Quan. “Robust Beamforming Design for Dual-Function Radar-Communication System”. In: *IEEE Transactions on Vehicular Technology* (2023).
- [37] Jing Xu et al. “Sparse Array Design for Joint Communication Radar System via Antenna Selection”. In: *2023 International Symposium on Signals, Circuits and Systems (ISSCS)*. 2023, pp. 1–4. DOI: 10.1109/ISSCS58449.2023.10190916.
- [38] Jing Xu et al. “Sparse Array Design for Joint Communication Radar System via Antenna Selection”. In: *2023 International Symposium on Signals, Circuits and Systems (ISSCS)*. 2023, pp. 1–4. DOI: 10.1109/ISSCS58449.2023.10190916.
- [39] Changhong Yu et al. “Cooperative localisation for multi-RSU vehicular networks based on predictive beamforming”. In: *Annals of Telecommunications* 79.1 (2024), pp. 85–100.